



HAL
open science

Post-functionalization of polyvinylcarbazoles: An open route towards hole transporting materials for perovskite solar cells

Camille Geffroy, Eftychia Grana, Muhammad Mumtaz, Ludmila Cojocaru, Eric Cloutet, Céline Olivier, Satoshi Uchida, Thierry Toupance, Hiroshi Segawa, Georges Hadziioannou

► **To cite this version:**

Camille Geffroy, Eftychia Grana, Muhammad Mumtaz, Ludmila Cojocaru, Eric Cloutet, et al.. Post-functionalization of polyvinylcarbazoles: An open route towards hole transporting materials for perovskite solar cells. *Solar Energy*, 2019, 193, pp.878-884. 10.1016/j.solener.2019.10.034 . hal-02330648

HAL Id: hal-02330648

<https://hal.science/hal-02330648>

Submitted on 2 Jul 2020

HAL is a multi-disciplinary open access archive for the deposit and dissemination of scientific research documents, whether they are published or not. The documents may come from teaching and research institutions in France or abroad, or from public or private research centers.

L'archive ouverte pluridisciplinaire **HAL**, est destinée au dépôt et à la diffusion de documents scientifiques de niveau recherche, publiés ou non, émanant des établissements d'enseignement et de recherche français ou étrangers, des laboratoires publics ou privés.

1
2
3
4
5
6
7
8
9
10
11
12
13
14
15
16
17

Post-functionalization of polyvinylcarbazoles: an open route towards hole transporting materials for perovskite solar cells

Camille Geffroy,^{a,b,c} Eftychia Grana,^a Muhammad Mumtaz,^a Ludmila Cojocaru,^c Eric Cloutet,^a Céline Olivier,^b Satoshi Uchida,^c Thierry Toupance,^{b,*} Hiroshi Segawa,^{c,*} and Georges Hadziioannou^{a,*}

^aLaboratoire de Chimie des Polymères Organiques, LCPO UMR 5629 CNRS, Université de Bordeaux, Bordeaux INP, Allée Geoffroy Saint-Hilaire, B8, F-33607 Pessac, Cédex, France. Email: georges.hadziioannou@enscbp.fr

^bInstitut des Sciences Moléculaires, ISM UMR 5255 CNRS, Université de Bordeaux, 351 Cours de la Libération, F-33405 Talence, Cédex, France. Email: thierry.toupance@u-bordeaux.fr

^cResearch Center for Advanced Science and Technology, University of Tokyo, 3-8-1 Komaba, Meguro-ku, Tokyo 153-8904, Japan. Email: cesgawa@mail.ecc.u-tokyo.ac.jp

Corresponding author: Thierry Toupance, thierry.toupance@u-bordeaux.fr

18 **Abstract**

19 We report on the potential of tuning poly(9-vinylcarbazole) (PVK) properties through
20 functionalization for an application as hole transport material (HTM) for perovskite solar cells
21 (PSCs). The synthesized PVK-based polymers were substituted with moieties of interest to
22 improve the solubility, the charge transport properties, or to tune energy levels. Bis(4-
23 methoxyphenyl)amine moieties were found to improve the hole mobility and to increase the
24 HOMO level of the PVK. Therefore, PSCs employing PVK-[N(PhOCH₃)₂]₂ as HTM exhibited
25 a best PCE of 16.7 %. Compared to spiro-OMeTAD, first studies have shown that PVK-
26 [N(PhOCH₃)₂]₂ could extend PSC lifetime.

27

28 **Keywords:** Polyvinylcarbazoles, Hole-transporting materials, Perovskite solar cells, Hole
29 mobility, Device stability.

30

31 **Highlights**

- 32 - Original synthesis of a new poly(9-vinylcarbazole) derivative hole transporting
33 material.
- 34 - Undoped or doped PVK-[N(PhOCH₃)₂]₂ showed hole mobility one order of magnitude
35 higher than undoped or doped spiro-OMeTAD, respectively.
- 36 - Used as hole transporter in n-i-p mesoscopic perovskite solar cells, PVK-
37 [N(PhOCH₃)₂]₂ yielded overall energy conversion efficiency up to 16.7%.
- 38 - Extended perovskite solar cell life-time using PVK-[N(PhOCH₃)₂]₂ as hole
39 transporting material without encapsulation.

40

41

42 1. INTRODUCTION

43 Organic-inorganic hybrid perovskite solar cells (PSCs) have attracted growing interest due to
44 an unprecedented increase in power conversion efficiency (PCE), which reached 24.2% within
45 less than ten years. [1-3] This outstanding advance is related to the remarkable optoelectronic
46 properties of lead halide perovskites, such as strong light absorption and long diffusion length
47 of the photogenerated charge carriers. [4-5] Moreover, processed from small quantities of
48 relatively cheap materials under mild conditions, PSCs are deemed to be a good alternative for
49 low-cost energy production and to be competitive with silicon solar modules. [6-7] However,
50 several hurdles have not entirely been overcome, especially the long-term stability of the
51 devices which is crucial for further industrialization of PSC modules. The device stability can
52 be altered by degradation of both materials and interfaces. Since the sensitivity of hybrid
53 perovskites towards moisture is known, many efforts have been devoted to enhance this
54 material's life-time for instance by tuning its composition or processing conditions. [8-10]

55 The HTM is another key material ruling both performance and stability of PSCs. Essential
56 for efficient extraction of holes, it also prevents the hybrid perovskite layer from ambient
57 humidity and degradation. The most studied and effective HTM reported so far is 2,2',7,7'-
58 Tetrakis[N,N-di(4-methoxyphenyl)amino]-9,9'-spirobifluorene known as *spiro*-OMeTAD.
59 However, due to burdensome synthesis and purification methods, this material is relatively
60 expensive. Moreover, its limited stability makes it unsuitable for industrial scale production.
61 [11] Therefore, new HTMs, either organic or inorganic, have been developed and investigated
62 to replace *spiro*-OMeTAD [11-12], such as molecular systems composed of spiro-like or
63 carboxylic-based cores [13], truxene-based core [14], nitrogen- or sulfur-containing central
64 scaffolds [13,15] or metallomacrocycles [13]. Some of them include small carbazole-based
65 molecules, like X51 and star-shape derivatives, which have been incorporated into PSCs. [16-
66 19] These materials showed similar properties to *spiro*-OMeTAD but their synthesis and

67 purification remain complicated limiting the quantities produced, and the solar cells involving
68 these HTMs still suffer from stability issues. On the other hand, poly(9-vinylcarbazole) (PVK)
69 is a p-type semiconducting polymer, commercially available and easily produced in large
70 quantities through controlled radical polymerization. [20] Due to its stability arising from its
71 polymeric backbone, hydrophobicity, large hole mobility and solution processability, PVK has
72 been widely used in organic electronic devices, as light emitting diodes [16] and organic solar
73 cells. [21-23] Recently, despite a relatively low HOMO level (-5.8 eV), PVK and PVK-based
74 polymers were successfully introduced in PSCs. Replacing PEDOT:PSS by a thin layer of PVK
75 led to a 15.8 % PCE in inverted structure. [24] PVK has also been used as an interlayer between
76 the perovskite and a triazatruxene-based HTM in order to enhance hole extraction and insulate
77 the perovskite layer from ambient moisture, thus leading to 18.8 % PCE. [25] Additionally, it
78 was recently shown that hyper-branched PVKs outperform P3HT in
79 ITO/TiO₂/perovskite/HTM/Ag structure. [26]

80 Moreover, several studies have shown the influence of ending groups of small molecules or
81 polymer units on the film forming and the optoelectronic properties of the HTMs. It has been
82 shown for instance that methoxy substituents improved the conductivity of carbazole-based
83 derivatives, [27] or that alkyl-ending chains could be introduced to enhance the solubility and
84 the film forming of thiophene-based HTMs. [28] On the other hand, bis(4-
85 methoxyphenyl)amine groups present in spiro-OMeTAD have been largely employed to design
86 new HTMs. [29, 30] The triphenylamine groups are reported to bring stability and good charge
87 transport properties to the materials. [31]

88 Herein, we report on the synthesis, the thorough characterization and the application as HTM
89 in PSCs of PVKs functionalized with diphenylamine (PVK-[N(PhOCH₃)₂]₂), *tert*-butyl (PVK-
90 (*t*Bu)₂) and methoxy (PVK-(OCH₃)₂) groups. Original post-functionalization routes of PVK
91 were thus established allowing a fine control of the molecular weight and a variety of

92 functionalization. This original method is more opened than conventional polymerization of
93 functional monomers. [32] Indeed, by contrast to the works reported by Xu *et al.* our
94 methodology is based on the preparation of well-defined PVK platforms that can be freely post-
95 functionalized. [32] The new materials were then tested in n-i-p planar and mesoscopic PSCs,
96 and the photovoltaic performances were rationalized in terms of conductivity and electronic
97 properties of HTMs.

98

99 **2. EXPERIMENTAL SECTION**

100 *2.1. Synthesis of poly[(3,6-di-methoxy)-9-vinylcarbazole] (PVK-[N(PhOCH₃)₂]₂)*

101 *2.1.1. Materials*

102 9-Vinylcarbazole (Aldrich, 98%) and AIBN (Azobisisobutironitrile, Acros 98 %) were
103 recrystallized from methanol. O-ethyl-S-(1-ethoxycarbonyl) ethyldithiocarbonate (C₈H₁₄S₂O₃)
104 was synthesized according to literature and used as the RAFT Chain Transfer Agent (CTA)
105 [33]. Tetrahydrofuran and toluene were purified through an MB-SPS-800 solvent purification
106 system and were stored under inert atmosphere before use. N,N-dimethylformamide (DMF,
107 99.8 %), dichloromethane (CH₂Cl₂, ≥ 99.9 %), methanol (CH₃OH, 99.8 %), ethanol
108 (CH₃CH₂OH, 99.8 %), acetonitrile (CH₃CN, 99.8 %), and dimethylsulfoxide ((CH₃)₂SO, 99.8
109 %) were purchased from Aldrich and used as received. 4,4'-Dimethoxydiphenylamine
110 (C₁₄H₁₅NO₂, 98 %) and sodium *tert*-butoxide (*t*-BuONa, 97 %) were purchased from ABCR,
111 tri-*tert*-butylphosphine ((*t*Bu)₃P, 98 %) and tris(dibenzylideneacetone)dipalladium(0),
112 (Pd₂(dba)₃) from Strem Chemicals, and N-bromosuccinimide (C₄H₄BrNO₂, 99 %) from Alfa
113 Aesar and were all used as received.

114

115 *2.1.2. Instrumentation*

116 ^1H and ^{13}C nuclear magnetic resonance (^1H -NMR and ^{13}C -NMR) spectra were recorded using
117 a Bruker AC-400 NMR at room temperature in deuterated chloroform (CDCl_3). Chemical shifts
118 (δ) for protons are reported in parts per million (ppm) downfield and are referenced to residual
119 proton in the NMR solvent (CHCl_3 ; δ 7.26 ppm). Size Exclusion Chromatography (SEC) was
120 performed on a Malvern Viscotek TDA 305 instrument equipped with viscometer, light
121 scattering (LS) and refractive index (RI) detectors with a 100A guard column and two PLgel
122 Mixed C bead columns assembled in series, in chloroform (CHCl_3) containing 1% triethylamine
123 as eluent with a flow rate of 1 mL/min at 30°C. The molecular weights of the polymers were
124 calculated through standard polystyrene (PS) calibration, as well as through universal
125 calibration. Fourier-transform infrared spectroscopy was performed on a Shimadzu IRAffinity-
126 1S, using the attenuated total reflection (ATR) method. Differential scanning calorimetry
127 (DSC) was performed on TA Instruments Q100 DSC system under helium flow (25 ml/min) at
128 a scan rate of 10°C/min, between 0°C and 250°C. Thermogravimetric analysis (TGA) data were
129 recorded on a TGA Q500 of TA Instruments using a heating rate of 10°C/min.

130

131 2.1.3. General procedure

132 2.1.3.1. PVK ($7 \text{ kg}\cdot\text{mol}^{-1}$)

133 In a typical experiment similar to literature, 12 g of 9-vinylcarbazole (VK, 62 mmol, 50 equ.),
134 0.27 g of O-ethyl-S-(1-ethoxycarbonyl) ethyldithiocarbonate (CTA, 1.2 mmol, 1 equ.) and 0.1
135 g of 2,2'-Azobis(2-methylpropionitrile) (AIBN, 0.6 mmol, 0.5 equ.) were mixed in 31 mL
136 tetrahydrofuran (THF, 40% w/v) in a 100 mL schlenk flask equipped with a magnetic stirrer
137 [33]. After 3 freeze-vacuum-thaw cycles, the mixture was stirred under nitrogen atmosphere at
138 60°C and the polymerization was stopped after 20h by dipping the polymerization flask into
139 liquid nitrogen. The polymer was precipitated in methanol, recovered by filtration and dried at
140 40°C for 24h to give 12 g of **PVK** (100 % yield). ^1H NMR (Fig. S1a) (400 MHz, CHCl_3) δ

141 (ppm) 7.8 – 5.7 (m, 7H), 5.3 – 4.5 (m, 1H), 3.5 – 2.9 (m, 1H), 2.1 – 0.9 (m, 2H) were identified
142 from the literature [34]. FTIR (Fig. S2) (ATR, 32 scans, cm^{-1}) 3100-3000 ar. C-H stretch, 3000-
143 2890 al. C-H stretch, 2300-1700 ar. C-H overtones, 1640-1070 skeletal vibrations al. and ar. C-
144 C, C=C stretch, 1060-860 C-H in-plane bending, and 800-650 C-H out-of-plane bending were
145 found.

146

147 2.1.3.2. PVK-Br₂

148 2 g of PVK ($7.0 \text{ kg}\cdot\text{mol}^{-1}$, 10 mmol, 1 equ.) were stirred with 103 ml DMF (1.9 % w/v) in a 250
149 mL round bottom flask until complete dissolution. 4.6 g N-bromosuccinimide ($\text{C}_4\text{H}_4\text{BrNO}_2$, 25
150 mmol, 2.5 equ.) in 26 mL DMF (17.8 %w/v) were added dropwise to the polymer solution after
151 cooling at 0°C. After addition, the mixture was stirred for 24h at room temperature under inert
152 atmosphere and then was precipitated in an excess of ethanol. Finally, the final product, **PVK-**
153 **Br₂**, was isolated through filtration and dried at 50°C under vacuum for 20h. The final mass
154 was 3.55 g (97.6% yield). FTIR (Fig. S2) (ATR, 32 scans, cm^{-1}) 3100-3000 ar. C-H stretch,
155 3000-2820 al. C-H stretch, 2100-1600 ar. C-H overtones, 1600-1000 skeletal vibrations al. and
156 ar. C-C, C=C stretch, 1470 asymmetric and 1270 symmetric, 1070-980 C-H in-plane bending,
157 900-540 C-H out-of-plane bending, 770-840 ar. C-H bend characteristic for aromatic
158 substitution, and 650 C-Br stretch were identified.

159

160 2.1.3.3. PVK-[N(PhOCH₃)₂]₂

161 Synthesis of poly[(3,6-diamine(N3,N3,N6,N6-tetrakis(4-methoxyphenyl)))-9-vinylcarbazole)
162 (PVK-[N(PhOCH₃)₂]₂) is based on Buchwald-Hartwig coupling reaction [35]. In a typical
163 experiment, 0.6 g of **PVK-Br₂** (1.7 mmol, 1 equ.) were stirred in a 250 mL round bottom flask
164 with 21.3 mL of toluene (2 wt.%) until dissolution under inert atmosphere. Then 0.05 g of tri-
165 tert-butylphosphine [(*t*-Bu)₃P, 0.3 mmol, 0.15 equ.], 0.12 g of

166 tris(dibenzylideneacetone)dipalladium(0) [Pd₂(dba)₃, 0.1 mmol, 0.07 equ.], 1.2 g of 4,4'-
167 dimethoxydiphenylamine (C₁₄H₁₅NO₂, 5.3 mmol, 3 equ.) and 0.5 g of sodium tert-butoxide (*t*-
168 BuONa, 5.3 mmol, 3 equ.) were added and the mixture was refluxed for 20h under N₂
169 atmosphere. The mixture was then poured over water and the final product was extracted into
170 dichloromethane. After removal of dichloromethane using a rotary evaporator, product was
171 diluted in small quantity of DMSO before precipitation in methanol. The obtained crude product
172 was purified through a Söxhlet procedure by washing with methanol, acetonitrile and toluene.
173 All Söxhlet fractions were dried at 50°C under vacuum for 24h. NMR analysis revealed that
174 the desired product, **PVK-[N(PhOCH₃)₂]₂** was that isolated from the toluene fraction. The final
175 mass was 0.5 g (45 % yield). ¹H NMR (Fig. S1b) (400 MHz, CHCl₃) δ 7.2 – 5.6 (m, 22H), 3.9
176 – 2.7 (m, 13H), 1.7 – 1.4 (m, 2H) were identified. FTIR (Fig. S2) (ATR, 32 scans, cm⁻¹) 3130-
177 3000 ar. C-H stretch, 3000-2770 al. C-H stretch (increased at 2800 because of –OCH₃ groups),
178 2300-1890 ar. C-H overtones, 1640-1070 skeletal vibrations al. and ar. C-C, C=C stretch, 1260-
179 1000 C-O stretch, 1000-860 C-H in-plane bending, and 800-650 C-H out-of-plane bending were
180 found.

181

182 **2.2. Perovskite solar cells**

183 **2.2.1. Materials**

184 Zinc powder, hydrochloric acid (HCl, 37 %), titanium diisopropoxide bis(acetylacetonate)
185 (TiAcAc, 75 wt.% in IPA), titanium(IV) chloride (99.9 %) and *tert*-butylpyridine (tBP, 96 %) were
186 purchased from Sigma Aldrich. Lead(II) chloride (PbCl₂, ultra dry, 99.999 %) was
187 obtained from Alfa Aesar, formamidinium iodide (FAI, > 99 %) and methylammonium
188 bromide (MABr, > 98 %) from Dyesol, magnesium(II) bis(trifluoromethanesulfonyl)imide
189 (Mg(TFSI)₂) from TCI, *spiro*-OMeTAD (99 %) from Merck and lithium bis(trifluoro-

190 methanesulfonyl) imide (LiTFSI) from Wako. The 24 nm nano-TiO₂ paste (PST-24NR) was
191 purchased from JPG C&C. Products were all used as received.

192

193 2.2.2. *n-i-p* planar device fabrication

194 FTO-glass substrates were patterned with zinc powder and HCl. Then, they were subsequently
195 washed through sonication in water and ethanol baths before being treated by UV-ozone
196 cleaner. A 50 nm-TiO₂ compact layer was deposited from a solution of TiAcAc in ethanol by
197 spray-pyrolysis at 400°C followed by annealing at the same temperature for 45 min. The
198 substrates were further immersed in a TiCl₄ solution in ethanol at 70°C before calcination at
199 500°C. CH₃NH₃I was synthesized according to a literature method [36]. CH₃NH₃I and PbCl₂
200 (3:1 molar ratio) were mixed in anhydrous DMF, deposited by spin coating at 2000 rpm and
201 annealed at 120°C for 45 min to form a dense perovskite layer of 330 nm. HTM solutions were
202 prepared by dissolving optimal concentration of *spiro*-OMeTAD (8 wt.%), PVK (5.9 wt.%),
203 PVK-[N(PhOCH₃)₂]₂ (4.3 wt.%), PVK-(*t*Bu)₂ (3.7 wt.%) and PVK-(OCH₃)₂ (3.1 wt.%) in 650
204 μL of chlorobenzene. LiTFSI and TBP, were necessary mixed to *spiro*-OMeTAD, PVK-
205 [N(PhOCH₃)₂]₂, PVK-(*t*Bu)₂ and PVK-(OCH₃)₂ to enhance hole extraction. Thus, 14 μL of 44
206 wt.% solution of LiTFSI in acetonitrile were added to the *spiro*-OMeTAD, PVK-(*t*Bu)₂ and
207 PVK-(OCH₃)₂ solutions, and 7 μL to the PVK-[N(PhOCH₃)₂]₂ solution. 20 μL of *t*BP were
208 added to all of the solutions. The HTMs were deposited by spin coating at 3000 rpm and let
209 overnight in dry air before finally evaporating an 80-nm thick gold electrode on top of the
210 device. **The thicknesses of the HTM layers were about 180 nm, 120 nm, 110 nm and 130 nm**
211 **for *spiro*-OMeTAD, PVK-(OCH₃)₂, PVK-(*t*Bu)₂ and PVK-[N(PhOCH₃)₂]₂ respectively.** In the
212 case of the undoped HTMs, the top electrode was made of 10 nm of MoO₃ and 80 nm of silver.
213 The device active area was 0.1 cm².

214

215 2.2.3. *n-i-p mesoscopic device fabrication*

216 FTO glass substrates were first laser etched and successively cleaned 10 min in ultrasonic bath
217 in water, detergent, acetone and ethanol, and by excimer UV cleaner. Then, a solution made of
218 TiAcAc mixed with 3 mol.% of LiTFSI and 3 mol.% of Mg(TFSI)₂ in ethanol was deposited
219 by spray pyrolysis at 430°C to form a 40-nm-compact-TiO₂ layer. The next steps were
220 performed in a dry room with dew point temperature at -30°C. A 150 nm mp-TiO₂ layer was
221 made by spin coating a solution of 24-nm-TiO₂ paste diluted in ethanol (14 wt.%), followed by
222 a 2-step annealing, at 125°C and 550°C. The layer was then doped with a LiTFSI solution in
223 acetonitrile (0.1 M) deposited by spin coating and annealed at 100°C and 430°C. Perovskite
224 precursor solution was made by dissolving MABr, PbBr₂, PbI₂ and FAI (1:1:5.75:5.45 mol) in
225 a mixture of DMSO and DMF (1:4 vol). 5 mol.% of KI, which was previously dissolved in
226 DMSO (1.5 M), were added to the perovskite solution. Anti-solvent spin-coating method was
227 carried out to make a dark, smooth and homogeneous perovskite layer which was annealed at
228 for 160°C. In the final process, a solution of FAI:MABr (5.45:1), **FAI or MABr** in isopropanol
229 was then deposited by spin-coating on top of the perovskite and rinsed with IPA before being
230 annealed at 80°C for 20 min. HTM solutions and films were prepared in the same conditions as
231 for the planar devices. Substrates were left overnight in the dry room. Finally, the 80-nm top
232 gold electrode was evaporated. The device active area was 0.181 cm².

233

234 2.2.4. *Characterizations*

235 UV/Vis absorption spectra were recorded on a Shimadzu UV-3600 spectrometer. Ionization
236 potentials were measured with a Riken Keiki AC-3 photoelectron spectrometer in air. Scanning
237 electron microscopy was performed on a Hitachi SU8000 system at 10 kV. Atomic force
238 microscope (Dimension FatScan, Bruker) was used in tapping mode to characterize HTMs
239 surfaces. I-V measurements were carried out with a solar simulator (CEP-25TF) under AM1.5G

240 solar light with an intensity of 100 mW.cm^{-2} calibrated by a standard silicon cell (BS-
241 520,S/N235). Reverse scan (from open-circuit to short-circuit) and forward scan (from short-
242 circuit to open-circuit) were recorded at a 100 mV.s^{-1} scan rate.

243

244 3. RESULTS AND DISCUSSION

245 3.1. Synthesis

246 The synthesis of PVK-[N(PhOCH₃)₂]₂ has required only three steps as depicted in Scheme 1.
247 First a well-defined PVK polymer of 7.0 kg.mol^{-1} was obtained through Reversible Addition
248 Fragmentation Transfer (RAFT) polymerization. Further bromination using N-
249 bromosuccinimide yielded the 3,6-bromo-functionalized PVKs. Finally, 4,4'-
250 dimethoxydiphenylamine substituents were introduced via Pd-catalyzed a Buchwald–Hartwig
251 reaction to give the target polymers PVK-[N(PhOCH₃)₂]₂ of 11.7 kg.mol^{-1} . On the other hand,
252 PVK-(*t*Bu)₂ was synthesized from PVK by Friedel-Crafts alkylation, whereas PVK-(OCH₃)₂
253 was prepared from PVK-Br₂ by direct displacement of bromine (Scheme 1). ¹H NMR and FTIR
254 analyses of all samples show a successful functionalization with the typical spectroscopic
255 features of the different moieties (Fig. S1 and S2). For instance, integration waves of the ¹H
256 NMR spectrum for PVK-[N(PhOCH₃)₂]₂ are consistent with the introduction of two N,N-di-p-
257 methoxyphenylamine groups (Fig. S1). The functionalization processes were also evidenced by
258 the evolution of the molar masses and the traces obtained by Size Exclusion Chromatography
259 (SEC) (Fig. S3) except for the *t*Bu-functionalized PVK that showed a multimodal distribution
260 (more probably due to interchain coupling during the chemical modification) and a small
261 discrepancy in ¹H NMR Integral values.. The macromolecular characteristics of the products
262 are summarized in Table 1. Moreover, it is worth underlining the simple purification procedure
263 used through Soxhlet extraction for PVK-[N(PhOCH₃)₂]₂, which facilitates the material
264 production and leads to moderate synthetic costs (Table S1). Due to the polymeric backbone

265 and the nature of the material, it is very easy to get rid of impurities and obtain a pure
266 functionalized polymer.

267

268 *3.2. Properties*

269 Polymer solubility was tested in polar and non-polar solvents at a concentration of 50 mg/mL
270 (Table S2). All polymers were soluble in chlorobenzene a suitable solvent to deposit HTMs in
271 PSCs. Besides, the dimethoxyphenylamine moieties of PVK-[N(PhOCH₃)₂]₂ improve the
272 solubility of PVK in several polar solvents.

273 Thermogravimetric analyses (TGA) indicate that the polymers are rather stable with a mass loss
274 lower than 10 % at 360°C (Fig. S4). Differential scanning calorimetry (DSC) evidences a lower
275 glass transition temperature of PVK (203°C) as compared to PVK-[N(PhOCH₃)₂]₂ (222°C) and
276 PVK-(OCH₃)₂ (219°C) (Fig. S5). It is worth mentioning that no transition was observed for
277 PVK-(*t*Bu)₂, and neither crystallization nor melting processes were observed for all materials
278 between 0 and 250°C.

279 The ionization potential and the band gap of the materials were measured from UV
280 photoelectron spectroscopy and UV-vis absorption and emission spectra (Table 1). HOMO
281 energy levels were estimated at -5.8, -5.1, -5.6 and -5.5 eV for PVK, PVK-[N(PhOCH₃)₂]₂,
282 PVK-(*t*Bu)₂ and PVK-(OCH₃)₂ respectively. The HOMO level of the PVK-[N(PhOCH₃)₂]₂
283 closely matches the valence band of the perovskites, estimated at -5.4 eV for MAPbI_{3-x}Cl_x and
284 -5.7 eV for K_{0.05}(MA_{0.15}FA_{0.85})_{0.95}PbI_{2.55}Br_{0.45}. [37, 38] “Hole-only” ITO/PEDOT:PSS (50
285 nm)/HTM (300 nm)/Au (50 nm) devices were fabricated. The dopants (*tert*-butylpyridine and
286 lithium bis(trifluoromethane-sulfonyl)imide) were used in the same proportions as for solar
287 cells fabrication. The current-voltage characteristics of the devices can be described by the
288 space-charge-limited current (SCLC) model. The hole mobilities were calculated from the
289 Mott-Gurney law (Table 2). *Spiro*-OMeTAD hole mobility was found to be around 10⁻⁶ cm².V⁻¹

290 $\text{cm}^2\text{V}^{-1}\text{s}^{-1}$, which is in the range of the values reported in the literature for these materials. [39, 40]
291 Methoxy and *tert*-butyl substitution resulted in a little decrease in hole mobility, while the
292 dimethoxyphenylamine substituted PVK was found to have an enhanced hole mobility, one
293 order of magnitude higher than that of *spiro*-OMeTAD. On the other hand, the hole mobility of
294 PVK-[N(PhOCH₃)₂]₂ was improved by two orders of magnitude, up to $1.7 \times 10^{-3} \text{ cm}^2\text{V}^{-1}\text{s}^{-1}$
295 upon the addition of LiTFSI and *t*BP. This is one order of magnitude higher than that found for
296 doped *spiro*-OMeTAD.

297

298 3.3. Photovoltaic properties

299 3.3.1. *n-i-p* planar perovskite solar cells

300 The performances of the synthesized PVK derivatives were first evaluated in archetypal
301 FTO/c-TiO₂/CH₃NH₃PbI_{3-x}Cl_x/HTM/Au planar PSCs. As expected, PVK, PVK-(*t*Bu)₂ and
302 PVK-(OCH₃)₂ exhibited very low PV performances due to their mismatching energy levels and
303 low hole mobility, with efficiencies not exceeding 2 % (Fig. S6). In contrast, a best PCE of
304 14.04 % was obtained employing PVK-[N(PhOCH₃)₂]₂. Compared to *spiro*-OMeTAD average
305 performances on 20 cells, PVK-[N(PhOCH₃)₂]₂-based PSCs exhibit comparable J_{sc} and reduced
306 V_{oc} for both scans, and enhanced FF in the case of the forward scan, leading to similar average
307 efficiency about 11.5 % (Fig. S7, Table S3). Hysteresis is often observed in TiO₂-based planar
308 devices and has been found to be partly caused by contact issues related to the lattice mismatch
309 of the TiO₂ and the perovskite. [41-43] Interestingly, replacing *spiro*-OMeTAD by PVK-
310 [N(PhOCH₃)₂]₂ reduced the hysteresis in planar devices.

311 The stability of the most efficient devices was evaluated by regularly measuring I-V curves
312 of *spiro*-OMeTAD and PVK-[N(PhOCH₃)₂]₂-based PSCs stored in different conditions: in inert
313 atmosphere (N₂ glovebox), in dry atmosphere, and in atmosphere with a relative humidity (RH)
314 about 20 % (Fig. 1). PSCs were kept in ambient light and ambient temperature without

315 encapsulation. In all cases, PVK-[N(PhOCH₃)₂]₂-based PSCs performed well and longer than
316 spiro-OMeTAD-based devices. Under nitrogen, PVK-[N(PhOCH₃)₂]₂-based PSC kept its
317 initial efficiency after 2 months while spiro-OMeTAD-based PSC exhibited around 65 % of its
318 initial efficiency. In dry atmosphere, efficiency of spiro-OMeTAD devices drastically
319 decreased from the day after its processing. The increase in efficiency for PVK-[N(PhOCH₃)₂]₂
320 could be attributed to the end of the evaporation of the remaining chlorobenzene used for the
321 HTM deposition and/or to the slow doping of the HTM through oxygen exposure. [44, 45] After
322 a 10-day experiment PCE was stable and slightly decreased after 2 weeks. Finally, in more
323 humid atmosphere, although spiro-OMeTAD PSC was slightly more stable than in dry
324 atmosphere, it achieved only around 30 % of its initial efficiency after 10 days, while the PVK-
325 [N(PhOCH₃)₂]₂-based device was around 65 %. This comparative study indicates the superior
326 stability of the planar PSCs using PVK-[N(PhOCH₃)₂]₂ as HTM.

327 Since dopants have been shown to be responsible for the poor stability of spiro-OMeTAD as
328 well as bubbles formed during the spin-coating deposition, topologies of pure and doped HTMs
329 were controlled by atomic force microscopy (AFM) (Fig. 2a, b). [46, 47] Homogeneous layers
330 were formed with pure materials. When adding dopants, no change in morphology was
331 observed for the polymer, whereas holes ($\varnothing \approx 50$ nm) appeared on top of the spiro-OMeTAD
332 layer. Same defects were observed in SEM cross-section images of freshly made spiro-
333 OMeTAD devices while in contrast, polymer layer remains homogeneous in 4-week aged
334 devices (Fig. 2c, d). In addition, contact angle measurements of a water drop in contact with
335 spiro-OMeTAD and the PVK-[N(PhOCH₃)₂]₂ films confirmed the higher hydrophobicity of the
336 polymer (Fig. 2e, f). Therefore, we postulate that the higher stability of the PVK-
337 [N(PhOCH₃)₂]₂-based devices may result from their better film-forming and covering of the
338 perovskite layer. The polymer is thought to act as a protective layer, insulating the hybrid
339 perovskite from the atmosphere and preventing the device from degradation.

340

341 3.3.2 *n-i-p mesoscopic perovskite solar cells*

342 The potential of the PVK-[N(PhOCH₃)₂]₂ as HTM was further studied in more efficient,
343 stable and reproducible *n-i-p* mesoscopic PSCs: FTO/bl-TiO₂/mp-TiO₂/K⁺ doped
344 MA_{0.15}FA_{0.85}PbI_{2.55}Br_{0.45}/HTM/Au. [33] The PVK-[N(PhOCH₃)₂]₂-based solar cells were
345 optimized by investigating the effect of the dopant concentration and the thickness on the PV
346 performances. The dopant concentration is noted as x:y:z, where x, y and z correspond to the
347 molar equivalence of the HTM, LiTFSI and tBP respectively. The reference doping ratio of
348 *spiro*-OMeTAD was 1:0.5:3.3. When increasing dopant concentration, V_{oc} was reduced and J_{sc}
349 and FF increased up to a maximum reached for the 1:1.25:8.25 dopant concentration (Table
350 S4). Thereby, PCE was improved from 11.93 to 14.49 %. For the next experiments, dopant
351 formulation was fixed at 1:1.25:8.25. The hole mobility of the doped polymer was 2.8 x 10⁻³
352 cm².V⁻¹.s⁻¹.

353 The thickness of PVK-[N(PhOCH₃)₂]₂ was then varied with the spin-coating parameters and
354 evaluated from the SEM cross section of the PSCs (Fig. S8). These images show the
355 homogeneity of the PVK-[N(PhOCH₃)₂]₂ layers, well covering the perovskite without pinholes.
356 Optimal PCE of 14.69 % was obtained for the 90-nm thick PVK-[N(PhOCH₃)₂]₂ (Table S5).

357 Despite optimizations of the layer, V_{oc} is still relatively low compared to planar PSCs. The
358 perovskite composition being different, it may locally modify the energy levels of the
359 perovskite or the interactions between the polymer and the perovskite at the interface. The
360 MA_{0.15}FA_{0.85}PbI_{2.55}Br_{0.45} perovskite contains an excess of lead. To make the perovskite/HTM
361 interface less lead rich, solutions of either FAI, MABr or FAI:MABr (0.85:0.15) were deposited
362 on top of the perovskite layer. All of the solutions had the effect to improve the V_{oc}, up to 1.07
363 V with MABr, and the PCE (Table S6). This may be due to a reduction of recombination at the
364 interface. A best PCE of 16.71 % with an acceptable hysteresis was achieved employing

365 **FAI:MABr**. Using a similar process, *spiro*-OMeTAD-based PSCs exhibited a best PCE of
366 **17.26 % with a lower FF and a higher V_{oc}** (Table 3, Fig. 3a). J_{sc} values extracted from EQE
367 measurements are in accordance with those deduced from I-V curves, with a slightly higher J_{sc}
368 in the case of *spiro*-OMeTAD (Fig. 3b). The maximum power point tracking (MPPT) of the
369 PSCs revealed a better stability in operating conditions and a better photoresponsivity of the
370 PVK-[N(PhOCH₃)₂]₂-based PSCs (Fig. 3c). In mesoscopic PSCs, PVK-[N(PhOCH₃)₂]₂
371 demonstrated high efficiencies and confirms its potential to improve the stability of PSCs.

372

373 **4. CONCLUSION**

374 To summarize, new poly(9-vinylcarbazole)s were synthesized through cost-effective post-
375 functionalization with different moieties. Bis(4-methoxyphenyl)amine ending groups increased
376 the HOMO level the PVK from -5.8 to -5.1 eV and improved the hole mobility over 10^{-3}
377 $\text{cm}^2/\text{V}\cdot\text{s}$ with the help of dopants. PVK-[N(PhOCH₃)₂]₂ HTM led to average photovoltaic
378 performances close to those of *spiro*-OMeTAD in n-i-p planar devices with a best achievement
379 of 14 % PCE **and extended lifetime**. In n-i-p mesoscopic devices the PCE was enhanced up to
380 16.7 %. More interestingly, the higher quality HTL is suggested to extend the planar device
381 lifetime, and to improve the stability of mesoscopic devices in operating conditions. These
382 results highlight the potentiality of the fine tuning of poly(9-vinylcarbazole) properties through
383 post-functionalization and open new directions to facilitate large-scale production at low cost
384 of high-efficiency PSCs.

385

386 **Acknowledgements**

387 This work was performed within the framework of LIA NextPV. IDEX Bordeaux is thanked
388 for PhD funding to CG. SU and HS thank Innovative energy technology international
389 collaborative investigation project, MITI, Japan. We are also thankful to ELORPrintTec ANR-

390 10-EQPX-28-01 and to LCPO/Arkema/ANR INDUSTRIAL CHAIR “HOMERIC” ANR-13-
391 CHIN-0002-01.

392 **Appendix A. Supplementary data**

393 Supplementary data related to this article can be found at <http://>

394

395

396 **References**

- 397 [\[1\] A. Kojima, K. Teshima, Y. Shirai, T. Miyasaka, Organometal halide perovskites as visible-](#)
398 [light sensitizers for photovoltaic cells, *J. Am. Chem. Soc.* 131 \(2009\) 6050–6051.](#)
- 399 [\[2\] J.-Y. Seo, H.-S. Kim, S. Akin, M. Stojanovic, E. Simon, M. Fleischer, A. Hagfeldt, S. M.](#)
400 [Zakeeruddin, M. Grätzel, Novel p-dopant toward highly efficient and stable perovskite solar](#)
401 [cells, *Energy Environ. Sci.* 11, \(2018\) 2448–2463.](#)
- 402 [\[3\] M. A. Green, Y. Hishikawa, E. D. Dunlop, D. H. Levi, J. Hohl-Ebinger, M. Yoshita, A. W.](#)
403 [Y. Ho-Baillie, Solar cell efficiency tables \(version 53\), *Prog. Photovolt. Res. Appl.* 27, \(2019\)](#)
404 [427–436.](#)
- 405 [\[4\] C. S. Ponseca, T. J. Savenije, M. Abdellah, K. Zheng, A. Yartsev, T. Pascher, T. Harlang,](#)
406 [P. Chabera, T. Pullerits, A. Stepanov, J. P. Wolf, V. Sundström, Organometal halide perovskite](#)
407 [solar cell materials rationalized: ultrafast charge generation, high and microsecond-long](#)
408 [balanced mobilities, and slow recombination, *J. Am. Chem. Soc.* 136 \(2014\) 5189-5192.](#)
- 409 [\[5\] S.D. Stranks, G. E. Eperon, G. Grancini, C. Menelaou, M. J. P. Alcocer, T. Leijtens, L. M.](#)
410 [Petrozza, H. J. Snaith, Electron-hole diffusion lengths exceeding 1 micrometer in an](#)
411 [organometal trihalide perovskite absorber, *Science* 342 \(2014\) 341-344.](#)
- 412 [\[6\] N.-G. Park, M. Grätzel, T. Miyasaka, K. Zhu, K. Emery, Towards stable and commercially](#)
413 [available perovskite solar cells, *Nat. Energy* 1 \(2016\) 16152-16159.](#)
- 414 [\[7\] M. Cai, Y. Wu, H. Chen, X. Yang, Y. Qiang, L. Han, Cost-performance analysis of](#)
415 [perovskite solar modules, *Adv. Sci.* 4 \(2016\) 1600269.](#)
- 416 [\[8\] N. Jeon, J. H. Noh, W. S. Yang, Y. C. Kim, S. Ryu, J. Seo, S. Il. Seok, Compositional](#)
417 [engineering of perovskite materials for high-performance solar cells, *Nature* 517 \(2015\) 476-](#)
418 [480.](#)
- 419 [\[9\] P. F. Ndione, W.-J. Yin, K. Zhu, S. Wei, J. J. Berry, Monitoring the stability of](#)
420 [organometallic perovskite thin films, *J. Mater. Chem. A* 3 \(2015\) 21940–21945.](#)
- 421 [\[10\] D. Bi, W. Tress, M. I. Dar, P. Gao, J. Luo, C. Renevier, K. Schenk, A. Abate, F. Giordano,](#)
422 [J.-P. Correa Baena, J.-D. Decoppet, S. M. Zakeeruddin, M. K. Nazeeruddin, M. Grätzel, A.](#)
423 [Hagfeldt, Efficient luminescent solar cells based on tailored mixed-cation perovskites. *Sci. Adv.*](#)
424 [2016, 2, e1501170.](#)

- 425 [\[11\] L. Calió, S. Kazim, M. Grätzel, S. Ahmad, Hole-transport materials for perovskite solar](#)
426 [cells, *Angew. Chemie Int. Ed.* 55 \(2016\) 2-26.](#)
- 427 [\[12\] A. Gheno, S. Vedraïne, B. Ratier, J. Bouclé, \$\pi\$ -Conjugated materials as the hole-](#)
428 [transporting layer in perovskite solar cells, *Metals* 6 \(2016\) 21.](#)
- 429 [\[13\] J. Urieta-Mora, I. Garcia-Benito, A. Molina-Ontoria, N. Martin, Hole transporting](#)
430 [materials for perovskite solar cells: a chemical approach, *Chem. Soc. Rev.* 47 \(2018\) 8541-](#)
431 [8571.](#)
- 432 [\[14\] L. Guan, X. Yin, D. Zhao, C. Wang, Q. An, J. Yu, N. Shrestha, C. R. Grice, R. A. Awni,](#)
433 [Y. Yu, Z. Song, J. Zhou, W. Meng, F. Zhang, R. J. Ellingson, J. Wang, W. Tang, Y. Yan, J.](#)
434 [Cost-effective hole transporting material for stable and efficient perovskite solar cells with fill](#)
435 [factors up to 82%, *Mater. Chem. A* 5 \(2017\) 23319-23327.](#)
- 436 [\[15\] S. Mabrouk, M. Zhang, Z. Wang, M. Liang, B. Bahrami, Y. Wu, J. Wu, Q. Qiao, S. Yang,](#)
437 [Dithieno\[3,2-b:2',3'-d\]pyrrole-based hole transport materials for perovskite solar cells with](#)
438 [efficiencies over 18%, *J. Mater. Chem. A* 6 \(2018\) 23319-23327.](#)
- 439 [\[16\] B. Xu, E. Sheibani, P. Liu, J. Zhang, H. Tian, N. Vlachopoulos, G. Boschloo, L. Kloo, A.](#)
440 [Hagfeldt, L. Sun, Carbazole-based hole-transport materials for efficient solid-state dye-](#)
441 [sensitized solar cells and perovskite solar cells, *Adv. Mater.* 26 \(2014\) 6629-6634.](#)
- 442 [\[17\] S. D. Sung, M. S. Kang, I. T. Choi, H. M. Kim, H. Kim, M. P. Hong, H. K. Kim, W. I.](#)
443 [Lee, 14.8% perovskite solar cells employing carbazole derivatives as hole transporting](#)
444 [materials, *Chem. Commun.* 50 \(2014\) 14161-14163.](#)
- 445 [\[18\] S. Benhattab, A.-N. Cho, R. Nakar, N. Berton, F. Tran-Van, N.-G. Park, B. Schmaltz,](#)
446 [Simply designed carbazole-based hole transporting materials for efficient solar cells, *Org.*](#)
447 [Electron. 56 \(2018\) 27-30.](#)
- 448 [\[19\] R. Nakar, A.-N. Cho, N. Berton, J. Faure-Vincent, F. Tran-Van, N.-G. Park, B. Schmaltz,](#)
449 [Triphenylamine 3,6-carbazole derivative as hole-transporting material for mixed cation](#)
450 [perovskite solar cells, *Chem. Papers* 72 \(2018\) 1779-1787.](#)
- 451 [\[20\] W. W. Limburg, D. J. Williams, Variation in inter-ring interactions in a series of carbazolyl](#)
452 [group containing polymers, *Macromolecules* 6 \(1973\) 787-788.](#)

453 [\[21\] M. Cai, T. Xiao, Y. Chen, E. Hellerich, R. Liu, R. Shinar, J. Shinar, Effect of molecular](#)
454 [weight on the efficiency of poly\(*N*-vinylcarbazole\)-based polymer light-emitting diodes, *Appl.*](#)
455 [Phys. Lett. 99 \(2011\) 203302.](#)

456 [\[22\] H.-S. Kim, C.-H. Kim, C.-S. Ha, J.-K. Lee, Organic solar cell devices based on](#)
457 [PVK/porphyrin system, *Synth. Met.* 117 \(2001\) 289-291.](#)

458 [\[23\] F. Deschler, D. Riedel, B. Ecker, E. Von Hauff, E. Da Como, R. C. I. MacKenzie,](#)
459 [Increasing organic solar cell efficiency with polymer interlayers, *Phys. Chem. Chem. Phys.* 15](#)
460 [\(2012\) 764-769.](#)

461 [\[24\] L. Yang, Y. Yan, F. Cai, J. Li, T. Wang, Poly\(9-vinylcarbazole\) as a hole transport material](#)
462 [for efficient and stable inverted planar heterojunction perovskite solar cells, *Sol. Energy Mater.*](#)
463 [Sol. Cells 163 \(2017\) 210-217.](#)

464 [\[25\] P.-Y. Su, L.-B. Huang, J.-M. Liu, Y.-F. Chen, L.-M. Xiao, D.-B. Kuang, M. Mayor, C.-Y.](#)
465 [Su, A multifunctional poly-*N*-vinylcarbazole interlayer in perovskite solar cells for high stability](#)
466 [and efficiency: a test with new triazatruxene-based hole transporting materials, *J. Mater. Chem.*](#)
467 [A 5 \(2017\) 1913–1918.](#)

468 [\[26\] Z.-G. Zhou, Y. Zhao, C. Zhang, D. Zhou, Y. Chen, Z. Lin, H. Zhen, Q. Ling, A facile one-](#)
469 [pot synthesis of hyper-branched carbazole based polymer as hole-transporting material for](#)
470 [perovskite solar cells, *J. Mater. Chem. A* 5 \(2017\) 6613-6621.](#)

471 [\[27\] A. Magomedov, S. Paek, P. Gratia, E. Kasparavicius, M. Daskeviciene, E. Kamarauskas,](#)
472 [A. Gruodis, V. Jankauskas, K. Kantminiene, K. T. Cho, K. Rakstys, T. Malinauskas, V.](#)
473 [Getautis, M. K. Nazeeruddin, Diphenylamine-substituted carbazole-based hole transporting](#)
474 [materials for perovskite solar cells: Influence of isomeric derivatives. *Advanced Functional*](#)
475 [Materials 2018, 28 \(9\), 1704351.](#)

476 [\[28\] I. Zimmermann, J. Urieta-Mora, P. Gratia, J. Aragón, G. Grancini, A. Molina-Ontoria, E.](#)
477 [Ortí, N. Martín, M. K. Nazeeruddin, High-efficiency perovskite solar cells using molecularly](#)
478 [engineered thiophene-rich, hole-transporting materials: Influence of alkyl chain length on](#)
479 [power conversion efficiency. *Advanced Energy Materials* 2016, 7 \(6\), 1601674.](#)

480 [\[29\] J. Zhang, B. Xu, L. Yang, C. Ruan, L. Wang, P. Liu, W. Zhang, N. Vlachopoulos, L. Kloo,](#)
481 [G. Boschloo, L. Sun, A. Hagfeldt, E. M. J. Johansson, The importance of pendant groups on](#)
482 [triphenylamine-based hole transport materials for obtaining perovskite solar cells with over](#)
483 [20% efficiency. *Advanced Energy Materials* 2017, 8 \(2\), 1701209.](#)

484 [\[30\] C. Huang, W. Fu, C.-Z. Li, Z. Zhang, W. Qiu, M. Shi, P. Heremans, A. K. Y. Jen, H. Chen,](#)
485 [Dopant-free hole-transporting material with a C_{3h} symmetrical truxene core for highly efficient](#)
486 [perovskite solar cells. *Journal of the American Chemical Society* 2016, 138 \(8\), 2528-2531.](#)

487 [\[31\] F. Zhang, S. Wang, H. Zhu, X. Liu, H. Liu, X. Li, Y. Xiao, S. M. Zakeeruddin, M. Grätzel,](#)
488 [Impact of peripheral groups on phenothiazine-based hole-transporting materials for perovskite](#)
489 [solar cells. *ACS Energy Letters* 2018, 3 \(5\), 1145-1152.](#)

490 [\[32\] Y. Xu, T. Bu, M. Li, T. Qin, C. Yin, N. Wang, R. Li, J. Zhong, H. Li, Y. Peng, J. Wang,](#)
491 [L. Xie, W. Huang, Non-conjugated polymer as an efficient dopant-free hole-transporting](#)
492 [material for perovskite solar cells, *ChemSusChem* 10 \(2017\) 2578–2584.](#)

493 [\[33\] H. Mori, M. Yahagi, T. Endo, RAFT polymerization of *N*-vinylimidazolium salts and](#)
494 [synthesis of thermoresponsive ionic liquid block copolymers, *Macromolecules* 42 \(2009\) 8082-](#)
495 [8092.](#)

496 [\[34\] A. Karali, G. E. Froudakis, P. Dais, F. Heatley, Carbon-13 nuclear magnetic relaxation](#)
497 [study of solvent effects on chain local dynamics of poly\(*N*-vinylcarbazole\) in dilute solution,](#)
498 [*Macromolecules* 33 \(2000\) 5524-5531.](#)

499 [\[35\] B. Xu, E. Sheibani, P. Liu, J. Zhang, H. Tian, N. Vlachopoulos, G. Boschloo, L. Kloo, A.](#)
500 [Hagfeldt, L. Sun, Carbazole-based hole-transport materials for efficient solid-state dye-](#)
501 [sensitized solar cells and perovskite solar cells, *Adv. Mater.* 26 \(2014\) 6629-6634.](#)

502 [\[36\] L. Etgar, P. Gao, Z. Xue, Q. Peng, A. K. Chandiran, B. Liu, M. K. Nazeeruddin, M. Grätzel,](#)
503 [Mesoscopic CH₃NH₃PbI₃/TiO₂ heterojunction solar cells, *J. Am. Chem. Soc.* 134 \(2012\)](#)
504 [17396-17399.](#)

505 [\[37\] P. Tonui, S. O. Oseni, G. Sharma, Q. Yan, G. Tessema Mola, Perovskites photovoltaic](#)
506 [solar cells: An overview of current status, *Renewable and Sustainable Energy Reviews* 91](#)
507 [\(2018\) 1025-1044.](#)

508 [\[38\] Z. Tang, T. Bessho, F. Awai, T. Kinoshita, M. M. Maitani, R. Jono, T. N. Murakami, H.](#)
509 [Wang, T. Kubo, S. Uchida, H. Segawa, Hysteresis-free perovskite solar cells made of](#)
510 [potassium-doped organometal halide perovskite, *Scientific Reports* 7 \(2017\) 12183.](#)

511 [\[39\] D. Shi, X. Qin, Y. Li, Y. He, C. Zhong, J. Pan, H. Dong, W. Xu, T. Li, W. Hu, J.-L. Brédas,](#)
512 [O. Bakr, Spiro-OMeTAD single crystals: remarkably enhanced charge-carrier transport via](#)
513 [mesoscale ordering, *Sci. Adv.* 2 \(2016\) e1501491.](#)

- 514 [\[40\] H. J. Snaith, M. Grätzel, Enhanced Charge Mobility in a Molecular Hole Transporter via](#)
515 [Addition of Redox Inactive Ionic Dopant: Implication to Dye-sensitized Solar Cells, Appl.](#)
516 [Phys. Lett. 89 \(2006\) 262114.](#)
- 517 [\[41\] B. Chen, M. Yang, S. Priya, K. Zhu, Origin of *J-V* hysteresis in perovskite solar cells, J.](#)
518 [Phys. Chem. Lett. 7 \(2016\) 905-917.](#)
- 519 [\[42\] H. S. Kim, N.-G. Park, Parameters affecting *I-V* hysteresis of CH₃NH₃PbI₃ perovskite solar](#)
520 [cells: effects of perovskite crystal size and mesoporous TiO₂ layer, J. Phys. Chem. Lett. 5 \(2014\)](#)
521 [2927-2934.](#)
- 522 [\[43\] L. Cojocaru, S. Uchida, P. V.V. Jayaweera, S. Kaneko, J. Nakazaki, T. Kubo, H. Segawa,](#)
523 [Origin of the hysteresis in I-V curves for planar structure perovskite solar cells rationalized with](#)
524 [a surface boundary induced capacitance model, Chem. Lett. 44 \(2015\) 1750-1752.](#)
- 525 [\[44\] U. Cappel, T. Daeneke, U. Bach, Oxygen-induced doping of spiro-MeOTAD in solid-state](#)
526 [dye-sensitized solar cells and its impact on device performance, Nano Lett. 12 \(2012\) 4925-](#)
527 [4931.](#)
- 528 [\[45\] E. J. Juárez-Pérez, M. R. Leyden, S. Wang, L. K. Ono, Z. Hawash, Y. Qi, Role of the](#)
529 [dopants on the porphological and transport properties of spiro-MeOTAD hole transport layer,](#)
530 [Chem. Mater. 28 \(2016\) 5702-5709.](#)
- 531 [\[46\] Z. Hawash, L. K. Ono, S. R. Raga, M. V. Lee, Y. Qi, Air-exposure induced dopant](#)
532 [redistribution and energy level shifts in spin-coated spiro-MeOTAD films, Chem. Mater. 27](#)
533 [\(2015\) 562-569.](#)
- 534 [\[47\] Y. Yue, N. Salim, Y. Wu, X. Yang, A. Islam, W. Chen, J. Liu, E. Bi, F. Xie, M. Cai, L.](#)
535 [Han, Enhanced stability of perovskite solar cells through corrosion-free pyridine derivatives in](#)
536 [hole-transporting materials, Adv. Mater. 48 \(2016\) 10738-10743.](#)

537

538

539 **Table 1.** Properties of the synthesized polymers.

Polymer	Theoretical M_n^a ($\text{kg}\cdot\text{mol}^{-1}$)	Experimental M_n vs PS standards ^b ($\text{kg}\cdot\text{mol}^{-1}$)	\bar{D}	E_g^d (eV)	E_{HOMO}^c (eV)	E_{LUMO}^f (eV)
PVK	9.880	6.980	1.4	3.6	- 5.8	- 2.2
PVK-Br ₂	17.770	c	c	c	c	c
PVK- [N(PhOCH ₃) ₂] ₂	32.610	11.730	1.4	2.6	- 5.1	- 2.5
PVK-(<i>t</i> Bu) ₂	15.050	8.500	1.6	3.4	- 5.6	- 2.2
PVK-(OCH ₃) ₂	12.440	8.500	1.2	3.1	- 5.5	- 2.4

540 ^a Theoretical calculation from $M_n = [\text{VK}]/[\text{CTA}] * M_n(\text{VK}) + M_n(\text{CTA})$. ^b vs. Polystyrene (PS) narrow standard
541 calibration SEC in chloroform/1% trimethylamine at 30°C. ^c Not measured. ^d Bandgap from absorption and
542 emission spectra. ^e HOMO level from photoelectron spectroscopy. ^f $E_{\text{LUMO}} = E_g + E_{\text{HOMO}}$.

543

544

545 **Table 2.** Hole mobility of pristine HTMs calculated from the Mott-Gurney law (average of 8
546 measurements).

	Hole mobility ($\text{cm}^2 \cdot \text{V}^{-1} \cdot \text{cm}^{-1}$)	
	Pure	Doped
<i>Spiro-OMeTAD</i>	$9.52 \pm 1.23 \cdot 10^{-7}$	$1.42 \pm 0.61 \cdot 10^{-4}$
PVK-(OCH₃)₂	$1.52 \pm 0.56 \cdot 10^{-7}$	$7.79 \pm 0.87 \cdot 10^{-7}$
PVK-(tBu)₂	$5.65 \pm 0.78 \cdot 10^{-7}$	$3.69 \pm 0.52 \cdot 10^{-7}$
PVK-[N(PhOCH₃)₂]₂	$1.43 \pm 0.68 \cdot 10^{-5}$	$1.67 \pm 0.32 \cdot 10^{-3}$

547

548

549

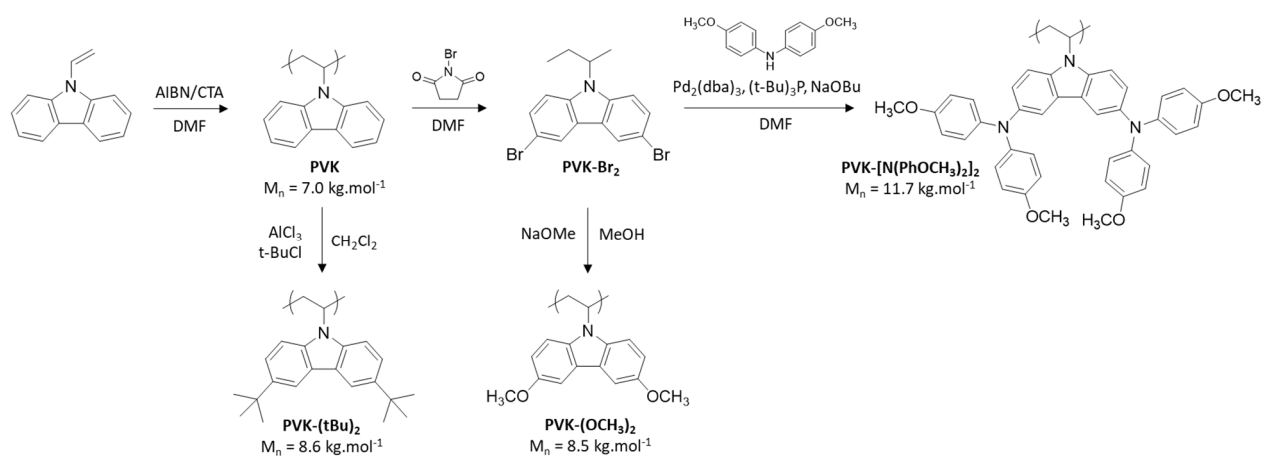
550 **Table 3.** Best and average (4 cells) PV performances of *spiro*-OMeTAD and PVK-
 551 [N(PhOCH₃)₂]₂-based n-i-p mesoscopic PSCs.

	Scan direction	V _{oc} (V)	J _{sc} (mA.cm ⁻²)	FF	PCE Average PCE (%)
<i>Spiro</i> -OMeTAD	Reverse	1.12	23.04	0.67	17.26 16.75 ± 0.45
	Forward	1.11	23.27	0.66	16.93 16.31 ± 0.53
PVK- [N(PhOCH ₃) ₂] ₂	Reverse	1.02	22.29	0.73	16.71 15.98 ± 0.49
	Forward	1.03	22.62	0.68	15.90 15.40 ± 0.34

552

553 **Scheme 1.** Synthetic routes towards PVK-(tBu)₂, PVK-(OCH₃)₂ and PVK-[N(PhOCH₃)₂]₂.

554



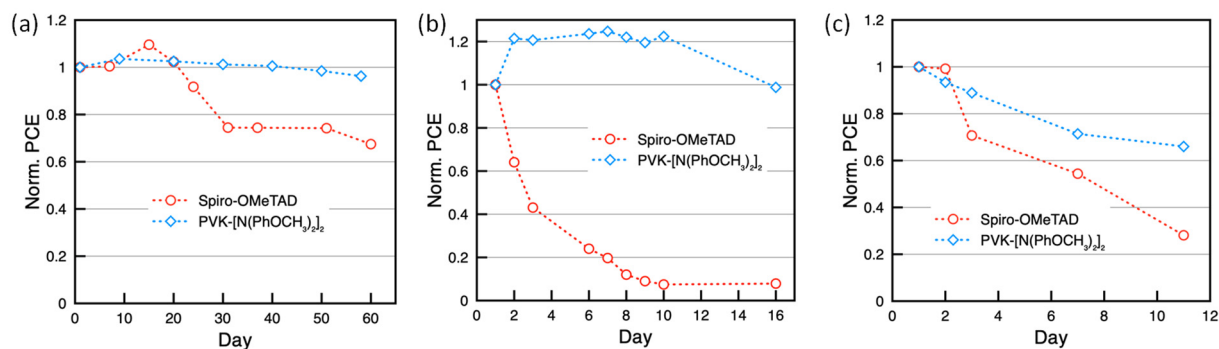
555

556

557

558 **Fig. 1.** Normalized PCE of n-i-p planar PSCs employing *spiro*-OMeTAD or PVK-
559 $[N(\text{PhOCH}_3)_2]_2$ as HTM stored in (a) glove box, (b) dry atmosphere ($\text{RH} < 2\%$) and, (c)
560 atmosphere ($\text{RH} \approx 20\%$).

561



562

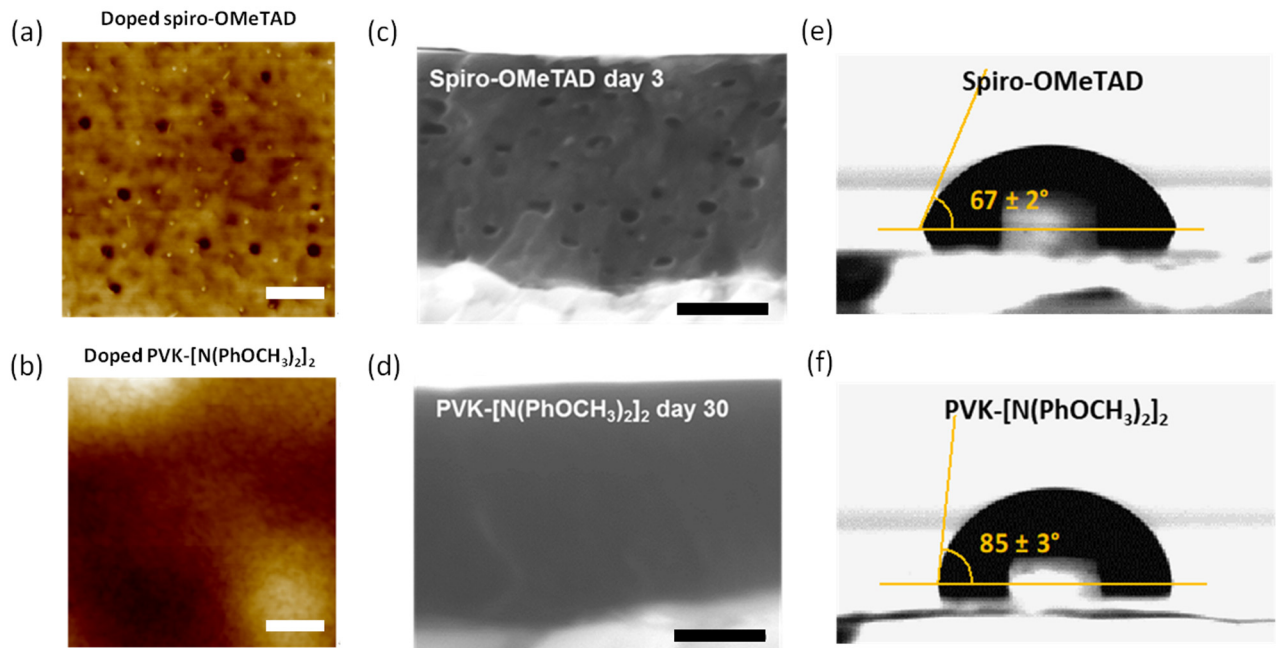
563

564

565

566 **Fig. 2.** AFM topographic views of HTM thin films on top of FTO/TiO₂/perovskite: (a) doped
567 *spiro*-OMeTAD and (b) doped PVK-[N(PhOCH₃)₂]₂. SEM cross sections of PSCs using as
568 HTM (c) *spiro*-OMeTAD after a 3-day ageing in dry room and (d) PVK-[N(PhOCH₃)₂]₂ after
569 a 30-day ageing in dry room. Scale bars = 200 nm. Contact angle measurement of a water drop
570 on (e) *spiro*-OMeTAD and on (f) PVK-[N(PhOCH₃)₂]₂ thin films.

571



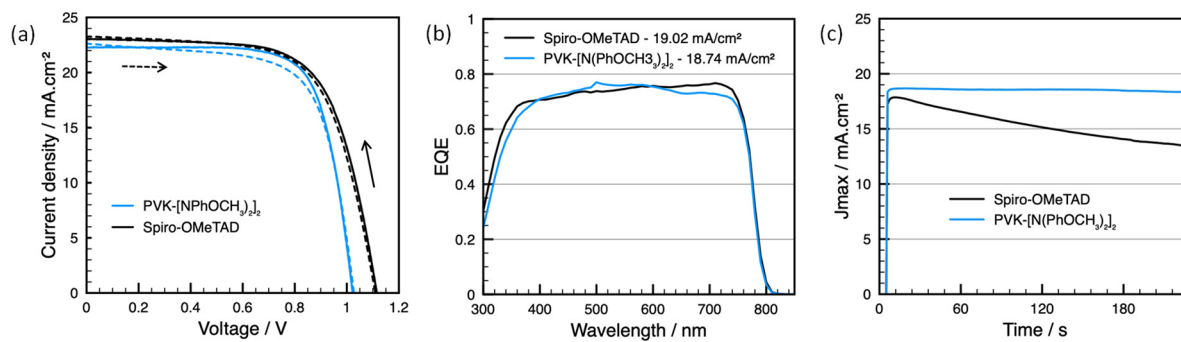
572

573

574

575 **Fig. 3.** Best J-V curves of n-i-p mesoscopic PSCs using *spiro*-OMeTAD or PVK-
576 $[N(\text{PhOCH}_3)_2]_2$ as HTM, (b) the corresponding EQE measurement and the integrated current
577 density, and (c) the maximum power point tracking.

578



579

580

Supplementary information

581

582

583 *Materials*

584 *tert*-Butyl chloride (C₄H₉Cl, 99 %) was purchased from Aldrich, copper(I)iodide (CuI, 99.99
585 %) from Strem Chemicals, sodium methoxide (CH₃NaO, 95 %) from Acros, aluminium
586 chloride (AlCl₃, 99 %) from Alfa Aesar and were all used as received.

587

588 *Synthesis of poly[(3,6-di-*tert*-butyl)-9-vinylcarbazole] (PVK-(*t*Bu)₂)*

589 Poly[(3,6-di-*tert*-butyl)-9-vinylcarbazole] was synthesized by Friedel-Crafts alkylation. 2 g of
590 **PVK** (7.0 kg.mol⁻¹, 0.2 mmol, 1 equ.) and 1.38 g of aluminum chloride (11 mmol, 1 equ.) were
591 stirred in dichloromethane (11 wt.%) in a 250 mL round bottomed flask at 0°C. 2.4 g of *tert*-
592 butylchloride (26 mmol, 2 eq.) were added within 90 min. The mixture was warmed to room
593 temperature and stirred overnight. Then, the reaction was cooled to 0°C in order to add 8 mL
594 of hydrochloric acid (33 %). The mixture was diluted with 28 mL of dichloromethane and
595 extracted twice with water and brine. The organic phase was dried over sodium sulfate. After
596 evaporation of the solvent, the polymer was dried overnight at 50°C to yield 2.4 g of **PVK-**
597 **(*t*Bu)₂** (78 % yield). ¹H NMR (Fig. S1b) (400 MHz, CDCl₃) δ 8.30 – 5.65 (m, 7H), 3.74 (dd, *J*
598 = 14.2, 7.5 Hz, 1H) and 2.13 – 0.24 (m, 14H) were identified. FTIR (Fig. S2) (ATR, 32 scans,
599 cm⁻¹) 3100-3000 ar. C-H stretch, 3000-2890 al. C-H stretch, 2300-1700 ar. C-H overtones,
600 1640-1070 skeletal vibrations al. and ar. C-C, C=C stretch, 1060-860 C-H in-plane bending,
601 and 800-650 C-H out-of-plane bending were found.

602

603 *Synthesis of poly[(3,6-di-methoxy)-9-vinylcarbazole] (PVK-(OCH₃)₂)*

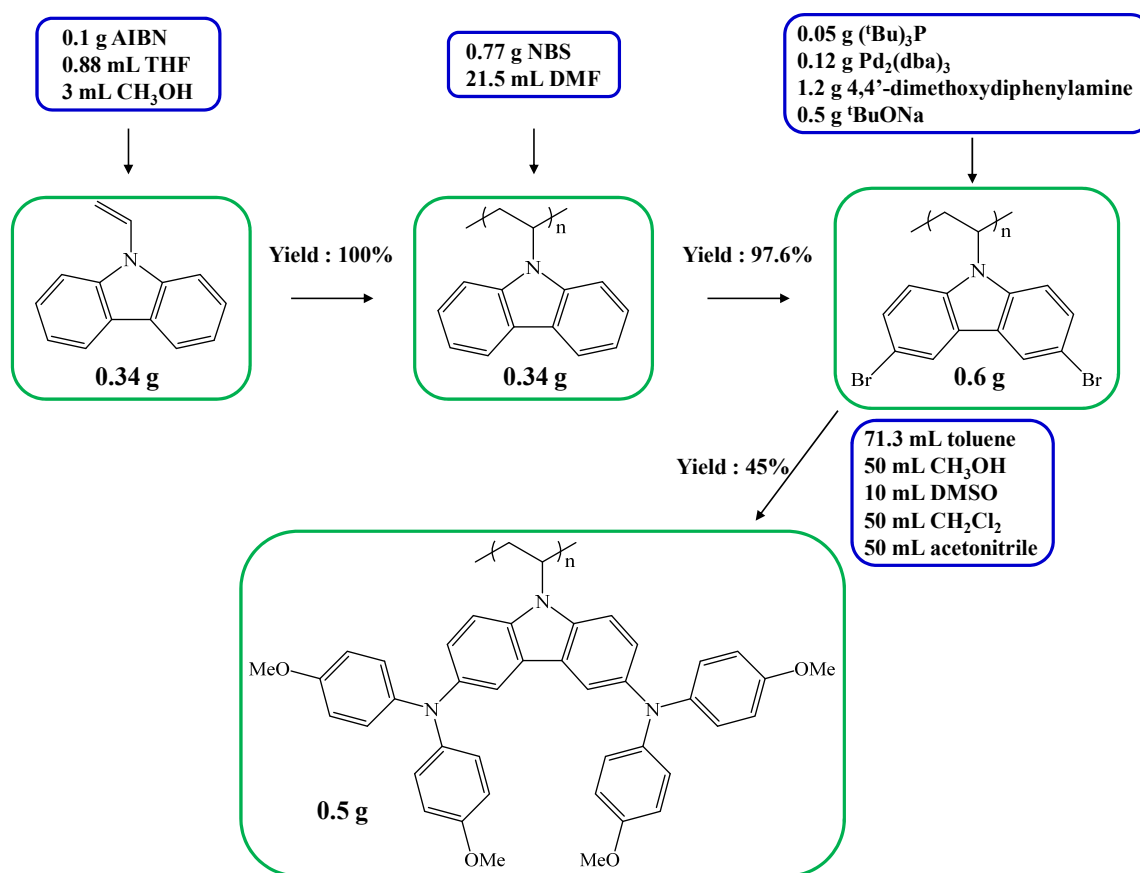
604 Poly[(3,6-di-methoxy)-9-vinylcarbazole] was synthesized from PVK-Br₂ by direct methoxide
605 displacement of bromine. First, 32 mL of sodium methoxide in methanol (25 wt.%) and 4.05 g

606 of copper bromide (28 mmol, 4 equ.) were added to 2 g of **PVK-Br₂** in 10 mL of DMF, 20 mL
607 of ethyl acetate and 20 mL of toluene in a 250 mL round bottomed flask. The reaction was
608 carried in inert atmosphere at 80°C for 24h. Then the mixture was poured over water, filtered
609 and washed with THF. Excess of solvents was evaporated. The left powder was resolubilized
610 in THF and precipitated in ethanol. Finally, filtration and drying overnight at 50°C led to 1.7 g
611 of **PVK-(OCH₃)₂** (75 % yield). ¹H NMR (400 MHz, THF) δ 8.89 – 5.40 (m, 7H), 3.76 (s, 3H)
612 and 2.92 – 1.01 (m, 2H) were identified. FTIR (Fig. S2) (ATR, 32 scans, cm⁻¹) 3100-3000 ar.
613 C-H stretch, 3000-2890 al. C-H stretch, 2300-1700 ar. C-H overtones, 1640-1070 skeletal
614 vibrations al. and ar. C-C, C=C stretch, 1260-1000 C-O stretch, 1060-860 C-H in-plane
615 bending, and 800-650 C-H out-of-plane bending were found.

616

617 Estimation of the synthesis cost of PVK-[N(PhOCH₃)₂]₂

618 Synthetic scheme:



619

620 Table S1: Synthesis cost to obtain 0.5 g of PVK-[N(PhOCH₃)₂]₂

Chemicals	Weight of reagent (g)	Price ^{a,b} (€/g)	Cost (€/g)
Vinyl Carbazole	0.34	2.04	0.694
AIBN	0.003	1.47	0.004
NBS	0.77	0.138	0.106
4,4'-dimethoxydiphenylamine	1.2	17	20.4
(tBu) ₃ P	0.05	31.9	1.60
Pd ₂ (dba) ₃	0.12	32.8	3.94
tBuONa	0.5	0.272	0.136
THF	0.78	0.009	0.007
CH ₃ OH	42	0.003	0.11
Toluene	61.8	0.002	0.15
DMF	20.3	0.085	1.73
DMSO	11	0.026	0.28
Dichloromethane	66.5	0.002	0.09
Acetonitrile	40	0.009	0.36

621 (a) For reagents, price from Aldrich, except (*t*Bu)₃P from from STREM chemicals, Pd₂(dba)₃ from
622 ABCR, and 4,4'-dimethoxydiphenylamine from TCI

623 (b) For solvents, price from VWR except DMF from Aldrich.

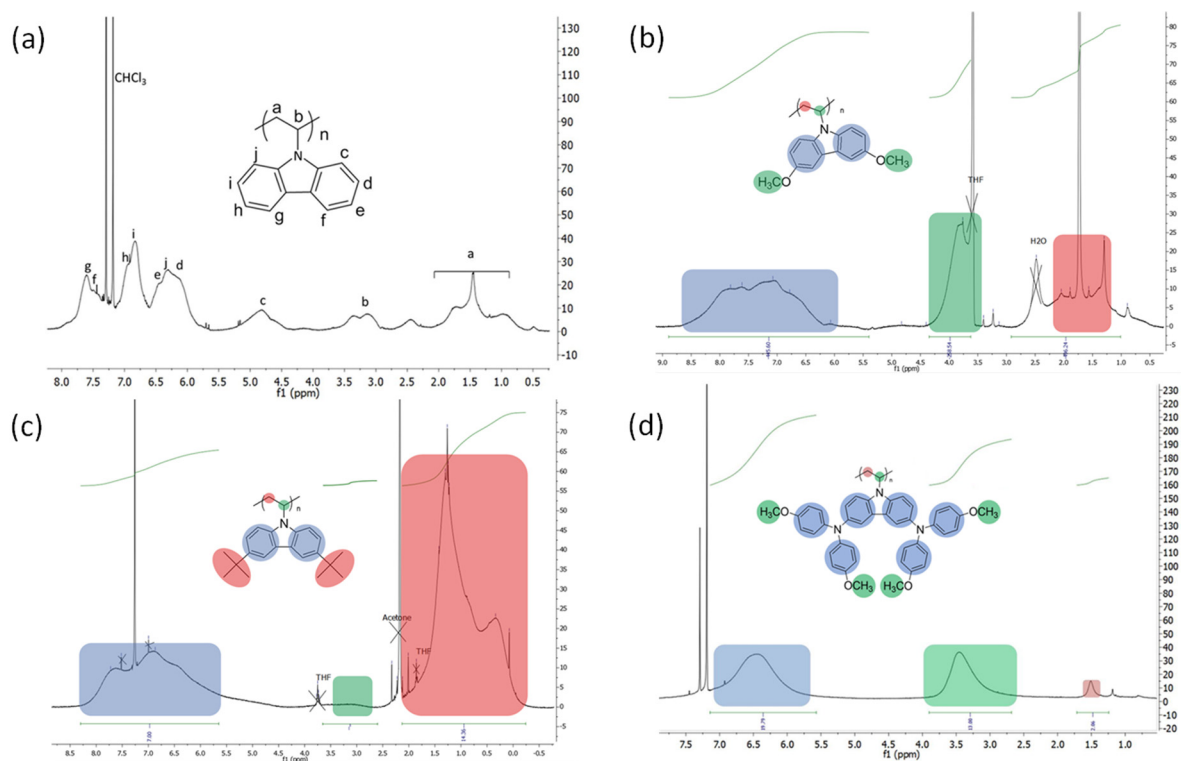
624

625 The cost for 1 g of PVK I was estimated to be about 59 €/g which is significantly lower than
626 spiro-OMeTAD (250 €/g Aldrich).

627

628

629



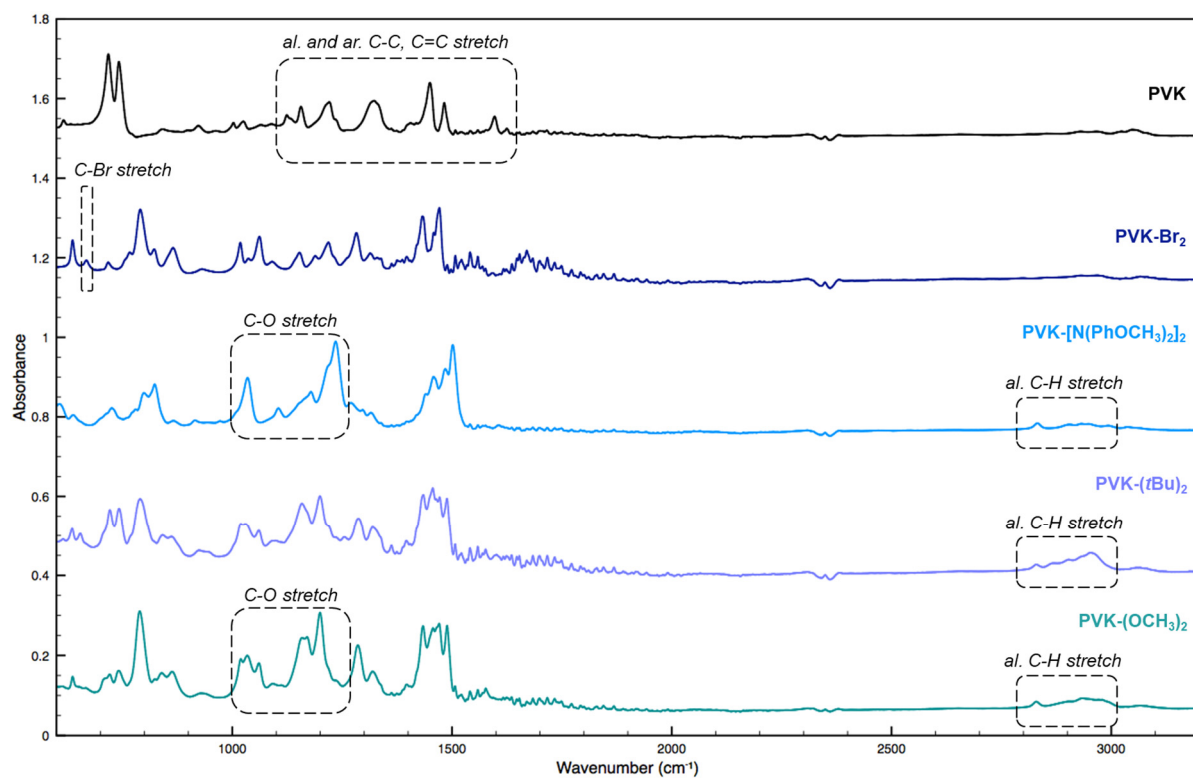
630

631

632 **Fig. S1.** ^1H NMR spectrum of (a) PVK, (b) PVK-(OCH_3) $_2$, (c) PVK-(tBu) $_2$ and (d) PVK- $[\text{N}(\text{PhOCH}_3)_2]_2$
 633 in chloroform-d.

634 The degree of functionalization for PVK- $[\text{N}(\text{PhOCH}_3)_2]_2$ was estimated from the integration
 635 wave of the ^1H NMR spectrum. Thus, for PVK- $[\text{N}(\text{PhOCH}_3)_2]_2$ the integration wave ratio
 636 between aromatic protons:methoxy + CH PVK:CH $_2$ PVK was found to be 10.7:6.7:1 which is
 637 very close to the one expected (11:6.5:1).

638

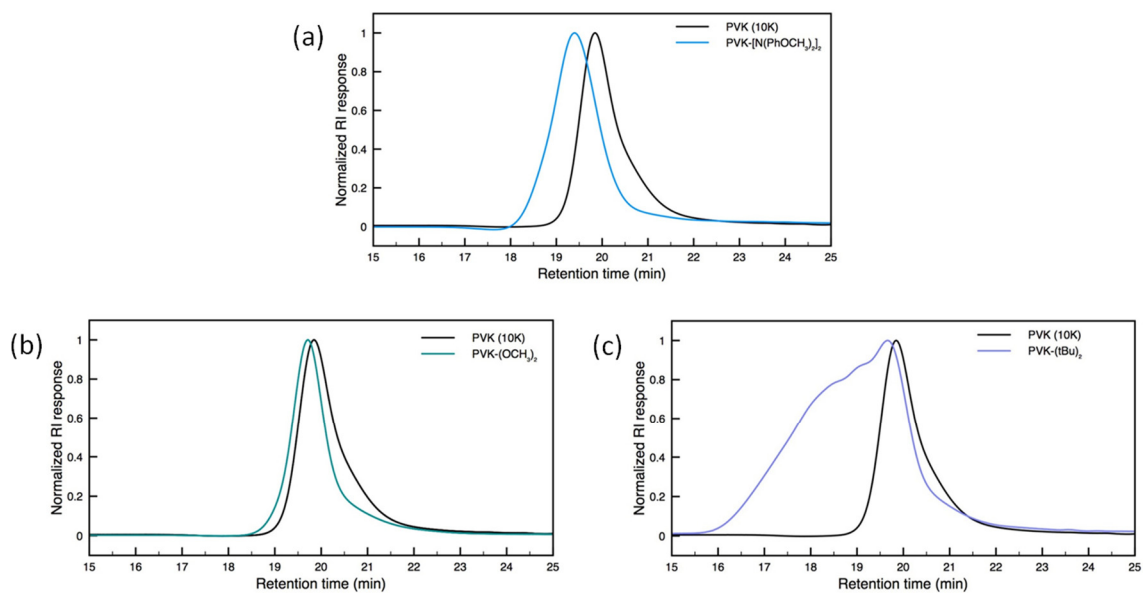


640

641 **Fig. S2.** FTIR spectra of PVK (black), PVK-Br₂ (dark blue), PVK-[N(PhOCH₃)₂]₂ (light blue), PVK-
642 (tBu)₂ (purple), and PVK-(OCH₃)₂ (green).

643

644



645

646 **Fig. S3.** SEC chromatograms (RI detector) in chloroform of PVK compared to (a) PVK-[N(PhOCH₃)₂]₂,
647 (b) PVK-(OCH₃)₂, and (c) PVK-(tBu)₂.

648

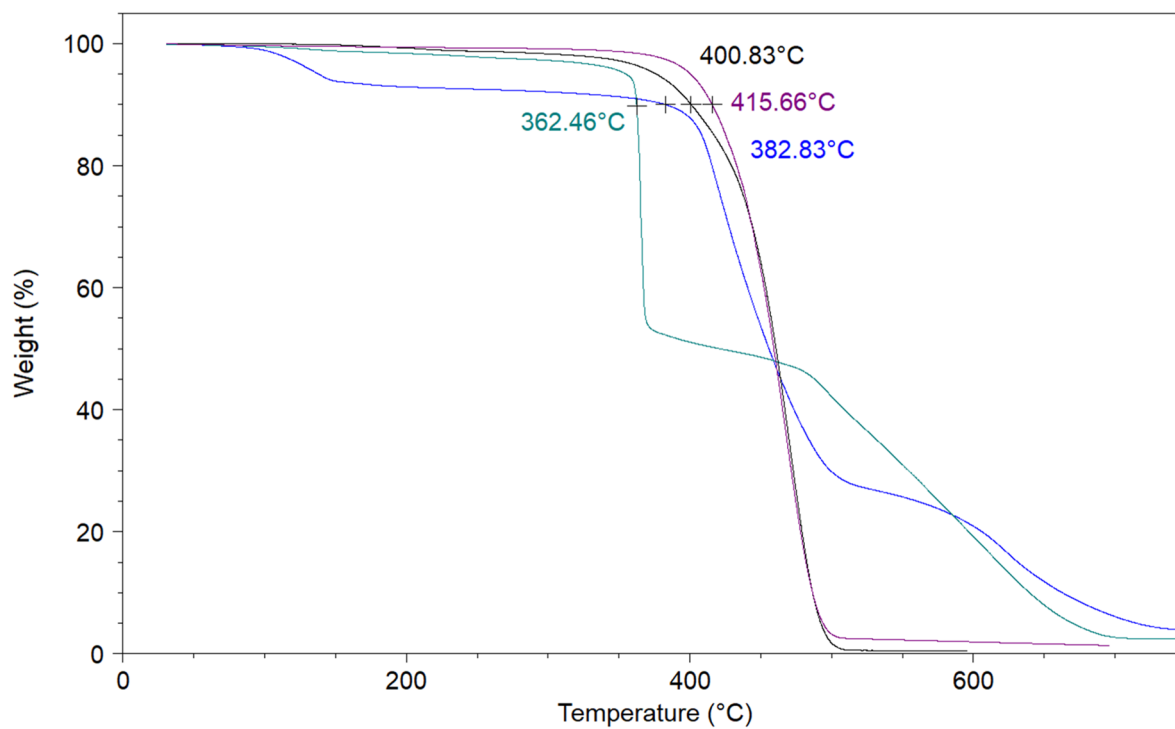
649 **Table S2.** Solubility of the polymers at 50 mg/mL.

Solvents	PVK	PVK-(OCH₃)₂	PVK-(tBu)₂	PVK- [N(PhOCH₃)₂]₂
Toluene	+	+	+	+
Chlorobenzene	+	+	+	+
Chloroform	+	+	+	+
Dichloromethane		+	+	+
Acetone	-	+	-	-
DMF		-	-	+
DMSO		-	-	+
Acetonitrile	-	-	-	+
Ethanol	-	-	-	-

650

651

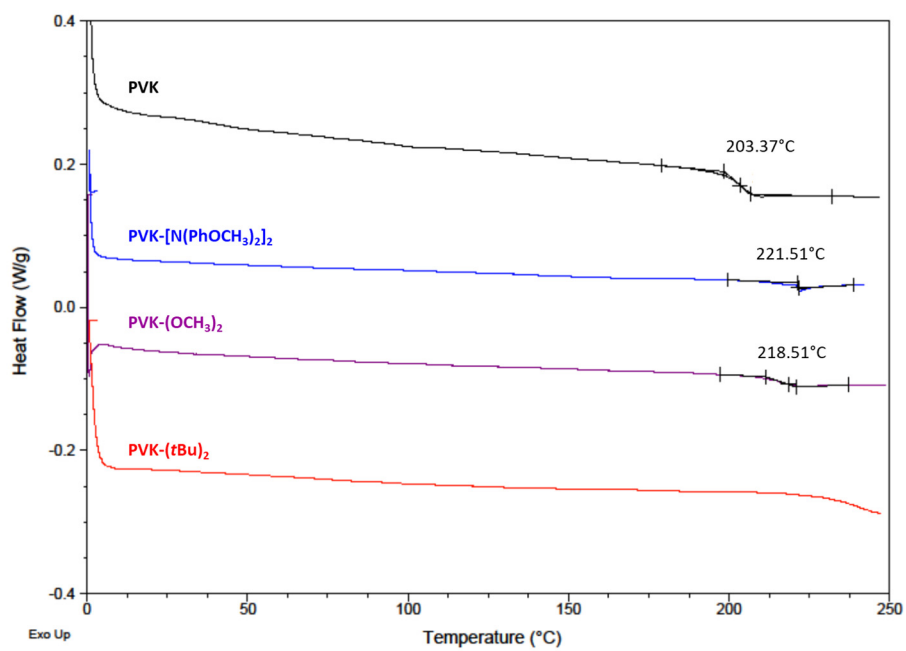
652



653

654

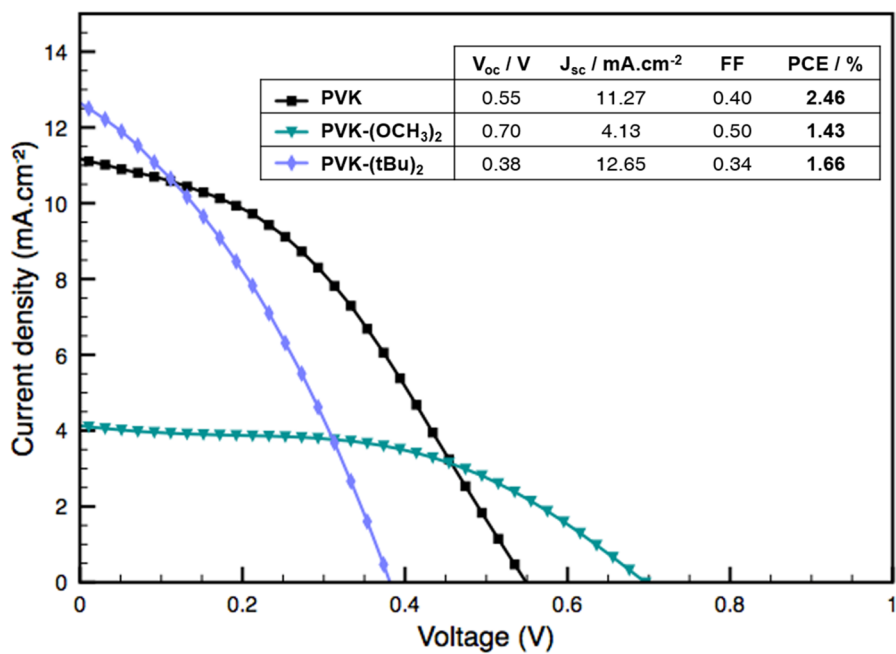
655 **Fig. S4.** TGA analysis and temperature at 10 % weight loss of the PVK and PVK-(tBu)₂ in ambient
656 atmosphere and, PVK-(OCH₃)₂ and PVK- N[Ph(OCH₃)₂]₂ in inert atmosphere.



657

658 **Fig. S5.** DSC scans and transition temperatures (T_g) of the PVK derivatives.

659

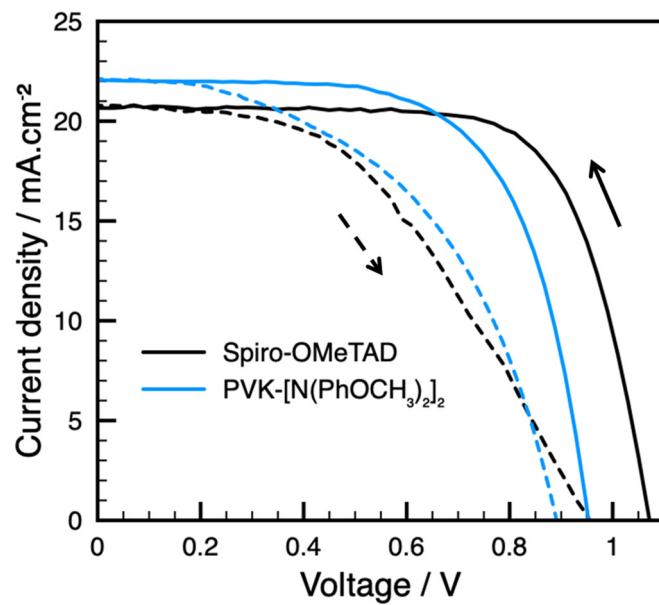


660

661

662 **Fig. S6.** Best I-V curves of n-i-p planar PSCs based on PVK, PVK-(OCH₃)₂ and PVK-tBu₂. Inset:
663 corresponding PV parameters.

664



665

666 **Fig. S7.** Best J-V curves of n-i-p planar PSCs using *spiro*-OMeTAD or PVK-[N(PhOCH₃)₂]₂ as HTM.

667

668 **Table S3.** Best and average (20 cells) PV performances of *spiro*-OMeTAD and PVK-[N(PhOCH₃)₂]₂-
 669 based n-i-p planar PSCs.

	Scan direction	V _{oc} (V)	J _{sc} (mA.cm ⁻²)	FF	PCE Average PCE (%)
<i>Spiro</i>-OMeTAD	Reverse	1.08	20.61	0.72	15.99 11.66 ± 2.13
	Forward	0.99	20.74	0.50	10.32 6.62 ± 2.94
PVK- [N(PhOCH₃)₂]₂	Reverse	0.95	22.05	0.67	14.04 11.30 ± 1.35
	Forward	0.89	22.07	0.50	9.89 6.14 ± 2.39

670

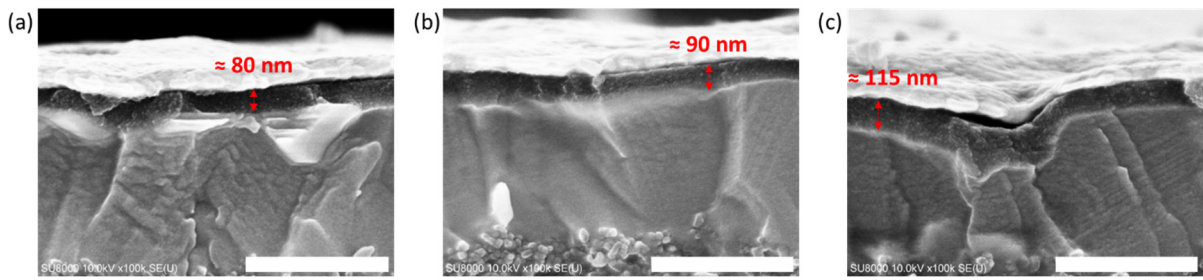
671

672 **Table S4.** Best and average (4 cells) PV parameters of PSCs using different dopant concentrations in
 673 PVK-[N(PhOCH₃)₂]₂.

Dopant concentration (HTM:LiTFSI:zBP)	Scan direction	J_{sc} (mA.cm ⁻²)	V_{oc} (V)	FF	PCE Average PCE (%)
1:0.25:1.65	Forward	19.62	0.99	0.51	10.04 9.03 ± 0.76
	Reverse	18.40	0.95	0.54	9.49 9.36 ± 0.68
1:0.5:3.3	Forward	19.55	0.99	0.59	11.27 10.76 ± 0.65
	Reverse	19.10	0.95	0.66	11.93 11.29 ± 0.50
1:0.75:4.95	Forward	19.88	0.91	0.71	12.69 11.59 ± 1.55
	Reverse	19.49	0.89	0.75	12.94 12.15 ± 1.15
1:1:6.6	Forward	21.31	0.86	0.73	13.44 13.52 ± 0.24
	Reverse	21.19	0.86	0.78	14.08 14.02 ± 0.20
1:1.25:8.25	Forward	21.87	0.90	0.73	14.40 14.45 ± 0.08
	Reverse	21.78	0.890	0.75	14.69 14.54 ± 0.05
1:1.5:9.9	Forward	21.65	0.86	0.72	13.32 12.56 ± 0.72
	Reverse	21.43	0.85	0.76	13.85 13.42 ± 0.33

674

675



676

677 **Fig. S8.** SEM cross-section images (10 kV) of polymer-based mesoscopic PSCs with different HTM
678 thicknesses. The darker layer is the HTM, the layer below is the perovskite and the top layer is the
679 gold electrode. Scale bar = 500 nm.

680

681 **Table S5.** Best and average (4 cells) PV parameters of PSCs according to PVK-[N(PhOCH₃)₂]₂
 682 thickness.

Thickness	Scan direction	J_{sc} (mA.cm ⁻²)	V_{oc} (V)	FF	PCE Average PCE (%)
80 nm	Forward	21.56	0.90	0.72	13.99 13.84 ± 0.22
	Reverse	21.33a	0.89	0.75	14.25 14.10 ± 0.17
90 nm	Forward	21.87	0.90	0.73	14.40 14.45 ± 0.08
	Reverse	21.78	0.890	0.75	14.69 14.54 ± 0.05
115 nm	Forward	22.24	0.894	0.73	14.46 14.22 ± 0.19
	Reverse	21.85	0.887	0.75	14.53 14.25 ± 0.21

683

684 **Table S6.** Best and average (4 cells) PV parameters of PSCs with modified perovskite/PVK-
 685 [N(PhOCH₃)₂]₂ interface.

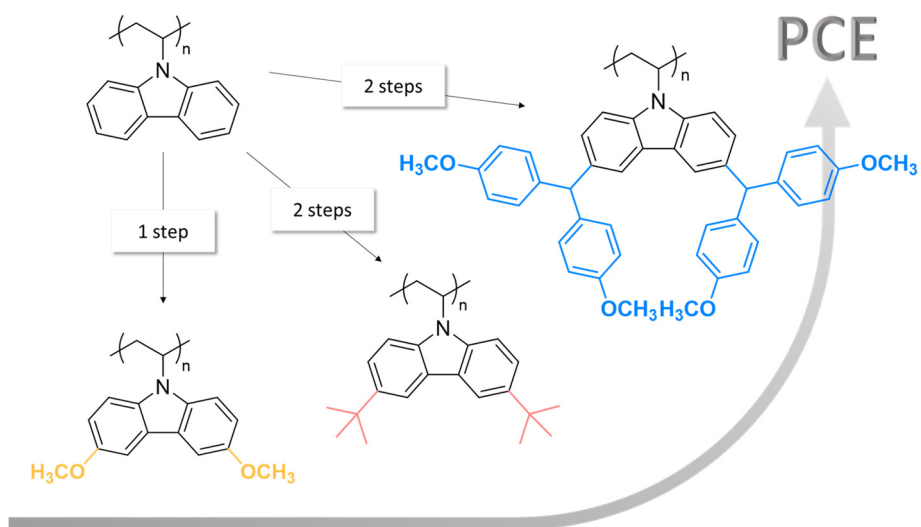
Salt	Scan direction	J_{sc} (mA.cm ⁻²)	V_{oc} (V)	FF	PCE Average PCE (%)
FAI	Reverse	22.86	0.93	0.73	15.50 14.95 ± 0.47
	Forward	23.26	0.94	0.71	15.45 14.86 ± 0.42
MABr	Reverse	20.64	1.066	0.69	15.13 14.70 ± 0.31
	Forward	20.98	1.055	0.64	14.27 13.85 ± 0.31
FAI:MABr (0.85:0.15)	Reverse	22.29	1.02	0.73	16.71 15.98 ± 0.49
	Forward	22.62	1.03	0.68	15.90 15.40 ± 0.34

686

687

Graphical abstract

688



689